UC-25 Metals, Ceramics, and Materials

WARD-3791-44

WELDING STAINLESS STEEL FUEL ELEMENT END PLUG CLOSURES

R. C. DeKlever
W. R. Jacoby
R. K. McGeary

Approved by: P. Murray
P. Murray

Contract AT(30-1)-4135
U. S. Atomic Energy Commission

Submitted to AEC-NYOO in February 1970

Westinghouse Electric Corporation
Advanced Reactors Division
P. O. Box 158
Madison, Pennsylvania 15663

Printed in the United States of America
Available from
Clearinghouse for Federal Scientific and Technical Information
National Bureau of Standards, U. S. Department of Commerce
Springfield, Virginia 22151
Price· Printed Copy $3.00; Microfiche $0.65

TABLE OF CONTENTS

Section	Title	Page
	ABSTRACT	vi
1	INTRODUCTION	1
2	EQUIPMENT	1
	2.1 Decontamination Chamber	1
	2.2 Welding Chamber	4
	2.3 Radiographic Inspection System	4
	2.4 Helium Leak Tester	5
3	MATERIALS	5
4	WELD JOINT DESIGN	5
5	WELDING DEVELOPMENT	8
	5.1 Welding Procedure	8
	5.2 Electrode Positioning	8
	5.3 Electrode Geometry	11
	5.4 End Plug Insertion	11
	5.5 Copper Deflector	11
	5.6 Effects of Random Variables	11
6	MATERIAL WELDABILITY	15
7	WELD DEFECTS	18
	7.1 Internal Solidification Voids	20
	7.2 Blow Holes	20
	7.3 Microfissures	20
	7.4 Seams and Underpenetration	20
	7.5 Inclusions	20
8	NONDESTRUCTIVE INSPECTION OF WELDS	22
	8.1 Visual and Radioactivity Monitoring	22
	8.2 Bubble Testing	22
	8.3 Radiography	22
	8.4 Helium Leak Testing	24
	8.5 Dye Penetrant Inspection	24
	8.6 Dimensional Inspection	24

TABLE OF CONTENTS

(Continued)

Section	Title	Page
9	CONCLUSIONS	24
10	ACKNOWLEDGEMENTS	24
	REFERENCES	26
	APPENDIX	27

LIST OF FIGURES

Figure		Page
1	EBR-II Type Irradiation Fuel Rod Assembly.....	2
2	Interior of the Decontamination Chamber.....	3
3	Top End Plug Used for EBR-II Type Irradiation Fuel Rods.....	7
4	Schematic Illustration Showing Effects of Electrode Position on Resulting Weld Nugget Geometry.....	10
5	Effects of Arc Voltage on Weld Nugget Geometry.....	12
6	Schematic of Arc Characteristics as Influenced by Electrode Tip Geometry.....	13
7	Weld Nugget Geometry as Influenced by Electrode Tip Configuration in 0.010 Inch Stainless Steel Tube-to-End Plug Welds.	14
8	Effects of Weld Metal Cooling Rates on Solidification Void Formation.....	16
9	Photomicrograph Showing Longitudinal Section of Weld Nugget Containing a Typical Internal Microfissure Associated with Solidification Void in 316 SS, 20% Cold Worked Tubing.....	17
10	Revised Schaeffler Constitution Diagram for Stainless Steel Weld Metal by W. T. DeLong.....	19
11	Photomacrograph Showing Transverse Section of a Tube to End Plug Closure Weld Illustrating the Circumferential Location of an Internal Solidification Void in the Weld Overlap Region...	21
12	Positive of a Weld Radiograph Illustrating an Acceptable Bottom End Closure Weld.....	23

LIST OF TABLES

Table		Page
1	Chemical Composition of Stainless Steel.....	6
2	Summary of GETR Phase I Weld Characterization Program.....	9

ABSTRACT

Liquid metal fast breeder reactor fuel elements typically consist of thin wall (circa 10 mils) stainless steel tubing containing uranium-plutonium ceramic fuel pellets. A TIG welding process was developed and used to fabricate experimental irradiation pins containing (U,Pu)C fuel immersed in sodium which required welding large stainless steel plugs inserted into the tube ends. Although this method has been adopted and applied by many laboratories, it is prone to the formation of defects attributable to non-uniform tube metal melting and soldification. Development results for solution annealed and 20% cold worked AISI 316 tubing are presented.

Discussion centers around the types and causes of the random defects that may occur for extensively refined procedures and equipment. The merits of various nondestructive and destructive testing methods for weld quality are presented. The importance of scrupulous adherence to parts dimensions, fitup, electrode configuration and positioning, and control of other process variables is illustrated.

1. INTRODUCTION

Extensive development work has been performed on welding equipment, variables which influence weld quality, material weldability, identification of weld defects, and related nondestructive and destructive inspection testing methods. These results evolved during the fabrication of experimental irradiation fuel rods used for thermal (GETR) and fast (EBR-II) neutron flux studies. Figure 1 illustrates a typical EBR-II type irradiation fuel rod assembly fabricated for irradiation testing.

Major problems encountered with welding of solution annealed and 20% cold worked AISI 304 and 316 stainless steel, 0.010 inch and 0.012 inch wall tubing were internal solidification voids, weld metal microfissuring, small blow holes, underpenetration, and seams. These welding defects could all be associated directly or indirectly with processing techniques or equipment limitations. Internal weld metal microfissuring was entirely associated with 20% cold worked, 316 stainless steel, 0.012 inch wall tubing. Refined procedures and strict process control applied to the welding process resulted in a high frequency of acceptable welds.

Nondestructive inspection methods such as visual examination, bubble testing, helium leak testing, dye penetrant testing, radiography, and dimensional inspection were used to determine final quality of all fuel rod weldments. Welding procedure qualification inspection consisted of all the aforementioned nondestructive inspection techniques. In addition, room temperature burst testing and metallography were used to evaluate mechanical and metallurgical properties of the tube to end closure welds. The welding development work expended during this contract culminated in documentation of a TIG welding specification which is presented in Appendix A.

An alternate method for the TIG process which appears to merit a feasibility study is plasma needle arc welding. This technique would not require the relatively strict control of arc gap and electrode tip geometry; in addition, tungsten inclusions would be eliminated.

2. EQUIPMENT

Equipment used for the welding and testing of the experimental irradiation test fuel rods consisted of a decontamination box, evacuable welding chamber, mass spectrometer helium leak detector, and a cabinet type x-ray machine.

2.1 Decontamination Chamber

After pellet loading from the fuel fabrication line, Tygon capped stainless steel tubing containing a preweighted slug of reactor grade sodium and (U,Pu)C fuel pellets was placed inside the decontamination chamber. The interior of the decontamination chamber is shown in Figure 2. A continuous, once-through inert gas purge technique was used to maintain the argon supplied within the chamber to less than 20 ppm oxygen and 10 ppm moisture. Oxygen and moisture contents were continuously monitored using a Westinghouse

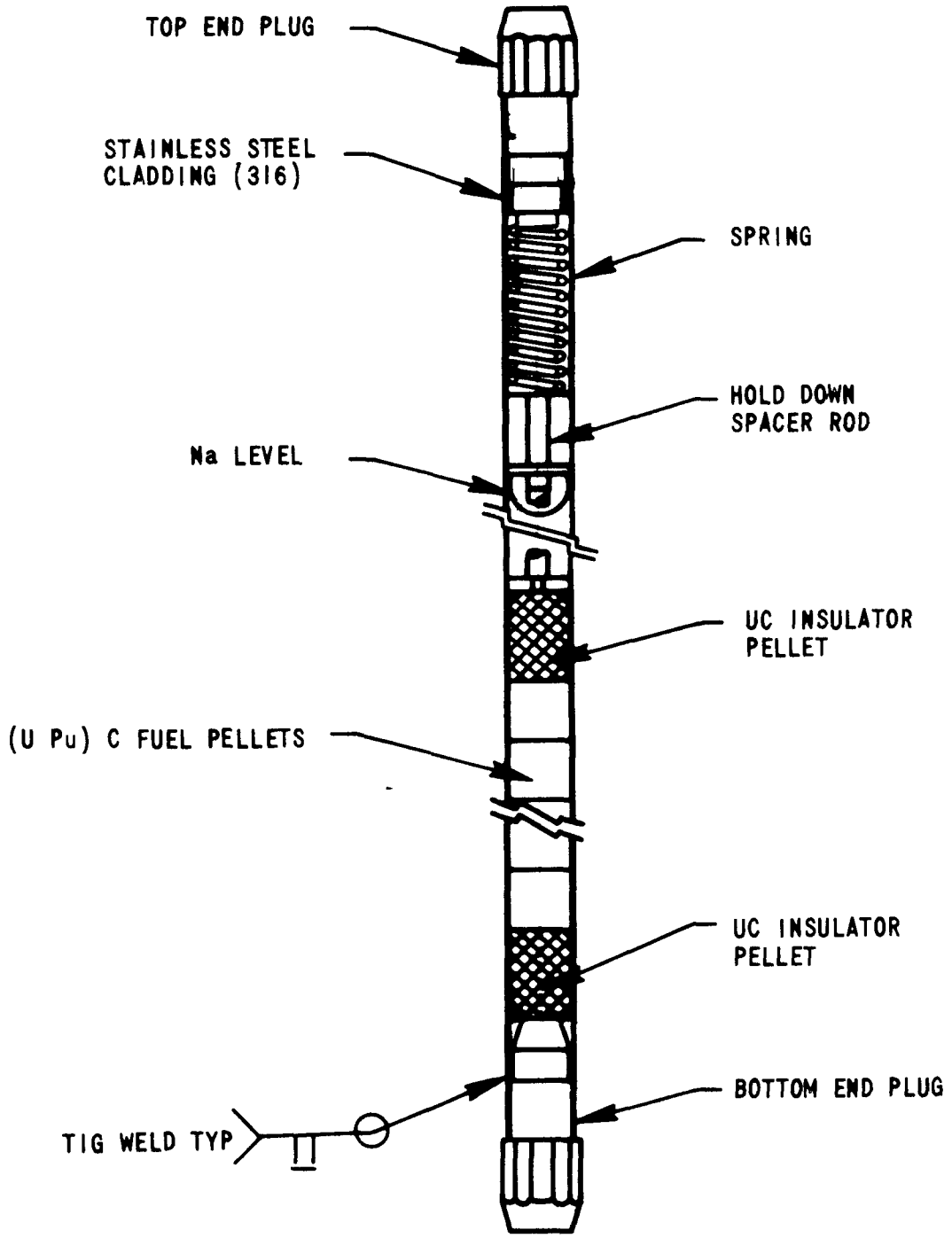

Figure 1 EBR-II Type Irradiation Fuel Rod Assembly

3462-1

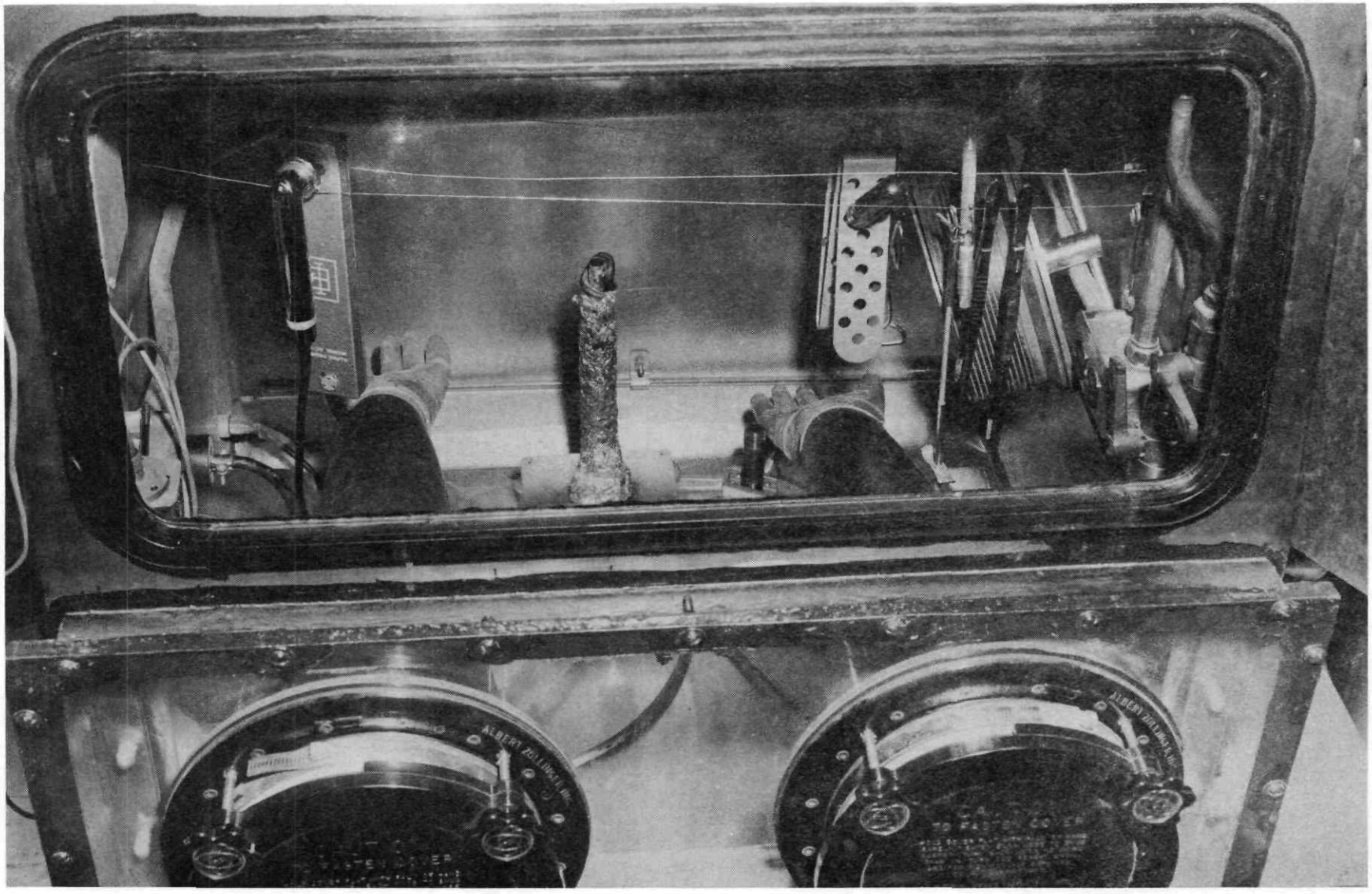

Figure 2 Interior of the Decontamination Chamber

model 207E electrolytic fuel cell oxygen analyzer and a Panametrics model 1000 probe type moisture monitor.

The Tygon cap was removed from each fuel rod, a stainless steel hold-down rod inserted, and a clean cap placed on the end of all fuel rods. Fuel rods were then individually placed in a preheated (500°F) hermetically sealed tubular furnace until all fuel pellets were completely immersed in sodium and at the bottom of the fuel rod. After cooling to room temperature, the open ended fuel tubes were decontaminated using dry cotton Q-tips, checked for evidence of gross contamination, recapped, and wiped with 200-proof ethyl alcohol. Fuel rods were then transferred into the welding chamber.

2.2 Welding Chamber

The welding chamber consisted of a 304 stainless steel square chamber with an internal volume of approximately 30 cubic feet. A suitable extension pipe mounted in the vertical direction allowed easy handling of the 28-1/2 inch long fuel rods during welding. The vacuum pumping system consisted of a protable CVC model PSE-42 which was capable of evacuating the chamber to $<1 \times 10^{-5}$ mm Hg.

The power supply used was a Miller ESR 150 amp D.C. welder with modular controls allowing precision set-up of the welding program cycle, i.e., initial start, weld cycle, and tail slope. In addition, the power supply was equipped with a high voltage capacitor discharge starting mechanism which allowed easy arc initiation in ultra-pure helium.

The drive mechanism consisted of a variable speed motor mounted externally to the vacuum chamber. Rotary motion was conveyed through the chamber wall with a suitable rotary vacuum seal. A Jacobs chuck mounted vertically within the chamber allowed various size tube diameters to be rotated with a high degree of precision. A Linde model HW-9 welding torch was attached to a jeweler's lathe compound slide rest which allowed for precise manual control of electrode-to-work (arc gap) settings.

Top end plug pressing of fuel bearing rods was accomplished inside the backfilled chamber using a modified calorimeter pellet press. The press was fitted with teflon hold-down pads which prevented damage to the thin wall cladding. Extensive modifications were required to allow accurate coaxial pressing of the spring loaded plug into the tube.

2.3 Radiography

Radiography of all fuel rod end closure welds was accomplished using a Field Emission Faxitron model 805 radiographic inspection system. This unit was capable of performing all radiography adequately at its maximum power output of 3 mA at 110 KVA.

2.4 Helium Mass Spectrometer

Helium leak detection was accomplished using a Veeco model MS-90-AB. Sensitivity levels of 1 x 10^{-10} atm-cc/sec. (1 part He in 1 x 10^{7} parts air) could be achieved.

3. MATERIALS

Fuel rod tubing consisted of AISI grade 304 and 316 stainless steel ordered to Westinghouse specification ARD-AMMA-001-1 and -2, respectively. End plug stock consisted of solution annealed type 316 stainless steel conforming to ASTM A276. Table 1 lists the chemical analysis, condition, and dimensions of materials used during development and actual irradiation pin fabrication. All material was air melted stainless steel; tubing was made by the seamless process.

Inspection of all tubing consisted of room temperature tensile, flattening, hydrostatic, intergranular corrosion, microstructure, penetrant, ultrasonic, and dimensional inspection.

4. WELD JOINT DESIGN

Fuel rod end closure joint design was determined by the necessary end plug configuration. Figure 3 illustrates the typical top end plug design used for fuel rod encapsulation prior to insertion into an EBR-II Mark A type capsule. Significant dimensions of the end plug are shown; a 0.001 inch nominal interference fit between end plug and the inside diameter of all tubes occurred along the 0.11 inch length of the end plug. Furthermore, a 0.002 inch maximum root radius was required at the end plug to tube end faying surfaces, assuring good joint fitup. Surface finish of end plug and tube ends was maintained at better than 32 AA. The spring, shown in Figure 1, was inserted prior to the top end plug, which resulted in a positive force of three to five pounds being exerted on the end plug during welding.

The end plug design has several unique advantages, which include mechanical and economic considerations. The structural model used assumed the end plug to be a rigid body with all deflections occurring by straining of the cladding. Stress calculations for this design at 1300°F resulted in a high margin of safety for local membrane and bending stresses. Peak stresses produced by stress concentration at the end plug to clad weld, assuming a 0.0075 inch weld fillet radius resulted in a fatigue stress concentration factor of 1.49 based on end-of-life conditions.[1]

This design lends itself to certain economic considerations from the standpoint of ease of manufacture, being suited for high rate screw machine processes.

Table 1. Chemical Composition of Stainless Steel (Wt. %)

Type	316[1]	316[2]	316[3]	304[4]
Condition	20% C.W.	Solution Annealed	Solution Annealed	Solution Annealed
Cr	17.62	17.48	17.59	18.75
Ni	13.19	12.65	12.52	9.87
Mo	2.24	2.29	2.89	.20
Mn	1.52	1.62	1.63	1.67
Si	.65	.42	.45	.40
Cu	.12	.21	.14	.25
Co	.11	.17	.23	--
N	.06	--	--	--
C	.055	.066	.059	.069
Nb	.03	--	--	--
Ti	.015	--	--	--
P	.018	.023	.023	.020
S	.015	.012	.026	.025
O	<.001	--	--	--
B	.0003	--	--	--
C/Si	1:12	1:6.5	1:7.5	1:5.8
Comments	Fuel Pin Cladding	Fuel Pin Cladding	End Plug Material	Fuel Pin Cladding

(1) Heat 20303 - Tube dimensions: 0.276" ± .0005 I.D. x 0.012" ± 0.0006 wall

(2) Heat 1914 - Tube dimensions: (a) 0.276" ± 0.0005" I.D. x 0.012" ± 0.0006" wall
(b) 0.230" ± 0.0005" I.D. x 0.010" ± 0.0005" wall

(3) Heat C-8522- End plugs machined from this stock

(4) Heat 1785 - Tube dimensions: 0.276" ± 0.0005"I.D. x 0.012" ± 0.0006"wall

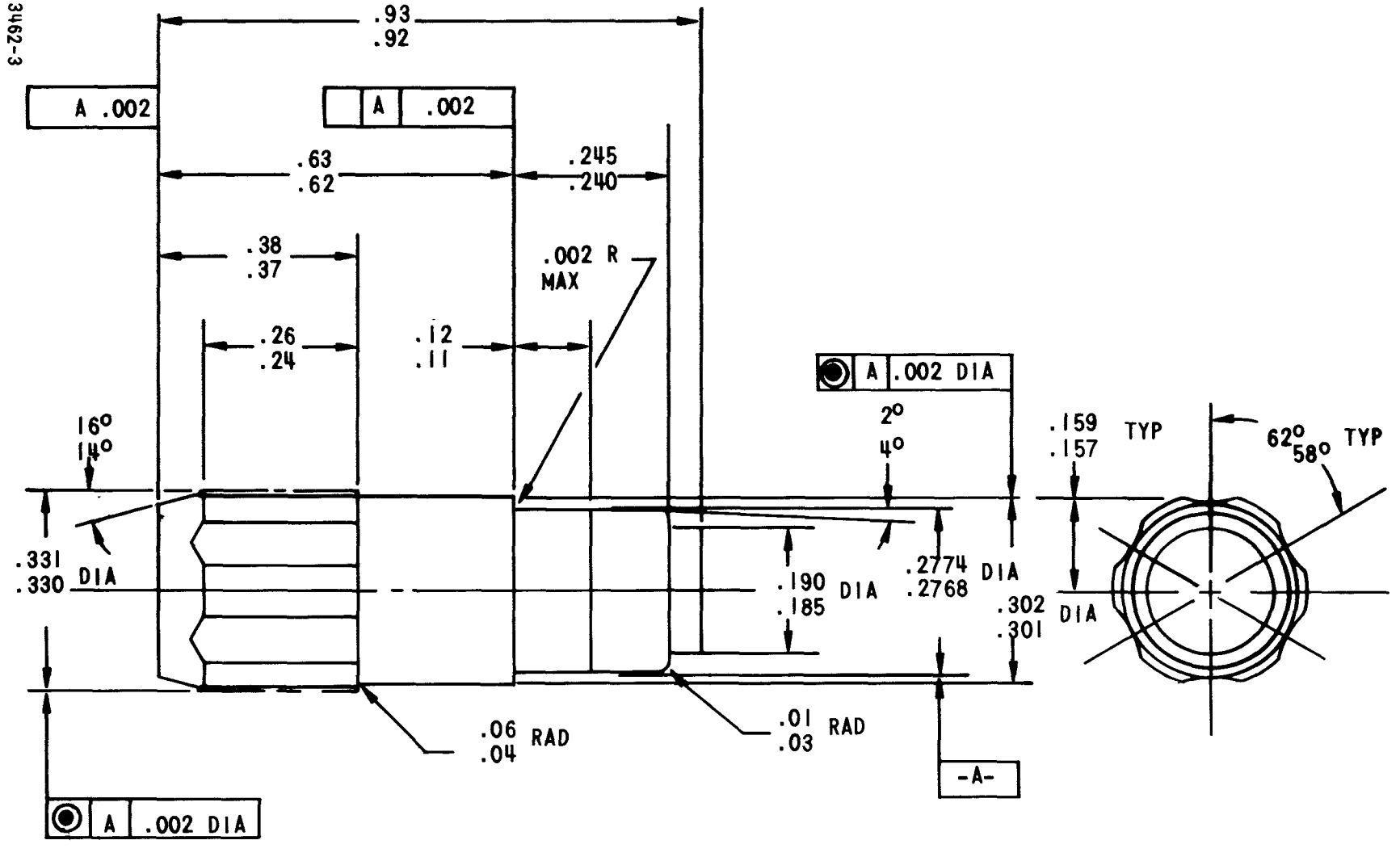

Figure 3 Top End Plug Used for EBR-II Type Irradiation Fuel Rods

5. WELDING DEVELOPMENT

Prior to the fabrication of irradiation test fuel rods extensive welding development work was performed to determine welding procedure, material weldability, weld metal properties, common weld defect types, and applicable nondestructive inspection techniques. All welding development was undertaken on reduced length samples made from identical tubing and end plug material used to fabricate the actual irradiation fuel rods. The inside and outside tube ends immediately adjacent to the weld area were lightly abraded using 600 SiC grit paper followed by a thorough chemical solvent cleaning; the end plugs were ultrasonically cleaned in acetone. Dimensional inspection was performed on all components. Critical operation on the tubing was ascertaining a minimum degree of ovality at the tube ends. Critical dimensions on the end plugs were the 0.002 inch maximum radius required at the weld joint to minimize seam gap and the inserted diameter which resulted in a 0.001 inch nominal diametrical interference fit in the tube.

5.1 Welding Procedure

Initial welding parameters, (i.e., welding amperage, arc gap, rotational speed, weld time, finish slope rate, electrode size, copper deflector placement, and electrode positioning) were established by metallographically sectioning and examining the resulting weld nuggets. All welding was performed in high purity helium with a total certified oxygen and nitrogen contamination level of <5 ppm. Since 100% weld penetration was required, the welding amperage was adjusted to achieve 150-200 percent penetration relative to the tubing wall thickness.

A welding program was initiated using 316 and 304 stainless steel tubing from heats 1914 and 1785, respectively, after establishing a satisfactory set of welding parameters. The results of the GETR Phase I weld characterization program presented previously[2] are shown in Table 2. These welds were made using a single pass technique and the random occurrence of detectable internal solidification voids and blow holes were relatively extensive. Room temperature burst test results for these samples indicated that all failures occurred in the tube wall and away from the weld area. Some of these samples contained internal solidification voids which reduced the tubing wall thickness up to 50% adjacent to the weld nugget. To refine the welding procedure further, additional study was directed to improving the precision of the welding equipment and further define the importance of the welding variables.

5.2 Electrode Positioning

Various electrode positions relative to the weld seam were evaluated. Figure 4 illustrates results for three different positions. For all development and actual pin fabrication welding the electrode tip was positioned as shown in Figure 4(b). Initial welding trials using a rack and pinion type torch holder resulted in random results caused by inadequacies in making fine adjustments. The rack and pinion holder was replaced with a compound two-dimensional jeweler's lathe slide. This device allowed for consistent positioning of the electrode within $\pm$ 0.001 inch of the desired location.

Table 2. Summary of GETR Phase-I Weld Characterization Program

	Tube Matl., Type SS, Heat 1785 & 1914	Visual Exam Bottom Weld (5x)	Visual Exam Bottom Weld (5x)	Leak Test (He)	Radiography Bottom Welds	Radiography Top Welds	Dye Penetrant Top/Bottom	Burst Press. @ Room Temp. (psig) Bottom Welds	Ulti. Burst Strength (x 10^3) psi	Location of Failure
1	304	✓	✓	✓	✓	✓	✓	7000	80.62	W
2	304	✓	✓	✓	✓	U	✓	7050	81.20	W
3	304	BH	✓	*	U	✓	✓/*	-	-	*
4	304	✓	✓	✓	U	U	✓	7100	81.76	W
5	304	✓	✓	✓	U	U	✓	7125	82.06	W
6	304	✓	✓	✓	✓	✓	✓	7100	81.76	W
7	304	✓	✓	CRACK	U	U	✓/*	-	-	*
8	304	✓	✓	✓	✓	U	✓	7100	81.76	W
9	304	✓	✓	✓	✓	✓	✓	7050	81.20	W
10	304	✓	✓	✓	✓	✓	✓	7175	82.64	W
11	316	✓	BH	*	U	U	*/✓	7750	89.30	W
12	316	✓	✓	✓	✓	✓	✓	7150	82.35	W
13	316	✓	✓	✓	✓	✓	✓	7125	82.06	W
14	316	✓	✓	✓	✓	U	✓	7025	80.91	W
15	316	✓	✓	✓	U	U	✓	7050	81.20	W
16	316	✓	✓	✓	U	✓	✓	7150	82.35	W
17	316	✓	✓	✓	U	U	✓	7550	86.97	W
18	316	BH	✓	*	U	✓	✓/*	7600	87.55	W
19	316	✓	BH	*	✓	U	*/✓	7600	87.55	W
20	316	✓	✓	✓	U	✓	✓	7150	82.35	W

✓ - Acceptable
BH - Blow Hole
* - Did not test
U - Indications of Internal Solidification Voids
W - Tube Wall

Notes: All end plug material is Type 316 SS, Heat C-8522.

All weld metal integrity was checked for cracks and voids at 150x, all were acceptable.

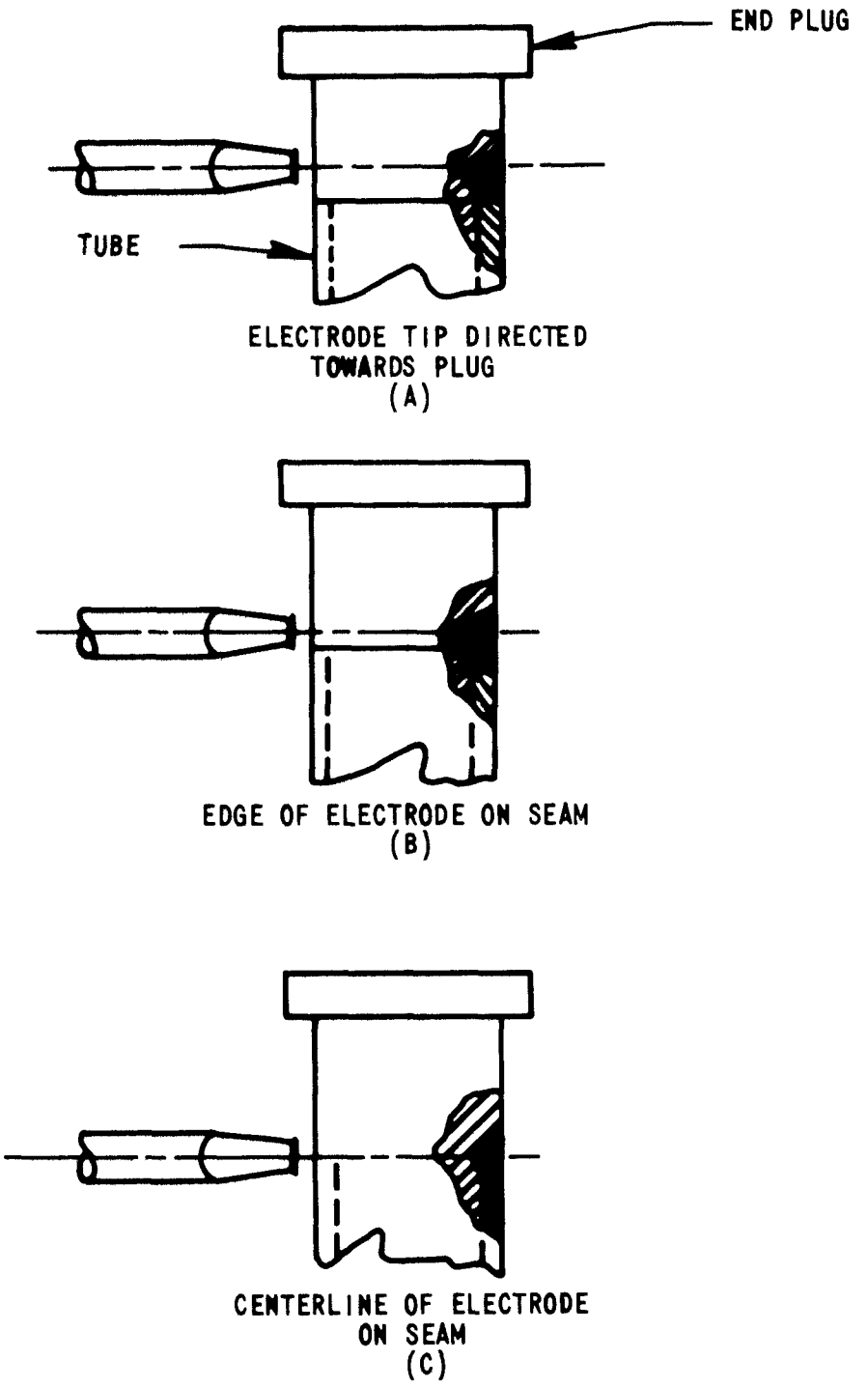

Figure 4 Effects of Electrode Position on Resulting Weld Nugget Geometry

3462-4

5.3 Electrode Geometry

The importance of electrode tip geometry was not apparent until major variations in weld nugget shape were noticed when using identical welding parameters. Many of the nuggets were shallow and wide instead of the desired narrow deep penetration welds. Lower arc voltage was found to contribute to desirable welds as shown in Figure 5. At D/W ratios [ratios of weld penetration (D) to weld width (W)] of less than about 0.25, tube wall melting and internal solidification voids become more pronounced. Variation in D/W ratios was found to be caused by corresponding variations in the effective plasma length of the arc. This condition is illustrated in Figure 6 for two different electrode tip shapes with equal arc gaps, but unequal effective plasma lengths. Measured arc voltage represents the sum of anode and cathode drops plus an incremental voltage drop proportional to plasma "climb" at the electrode tip. This climb increases the effective plasma length which increases the total arc voltage.[3] Figure 7 shows this effect on weld penetration where all welding parameters were constant. A newly ground electrode with a diameter/4 tip was used to produce a shallow nugget while a well-used blunt tip produced the deep weld nugget.

5.4 End Plug Insertion

Several plugs were deliberately started into tubes in a cocked position during insertion. Radiographs were taken before and after welding to correlate the amount of interface separation. Good correlation was obtained between detectable interface separation and internal solidification voids after welding. This is the result of poor heat transfer across the separated interface which caused excessive heat buildup and subsequent melting of these portions of the tube.

5.5 Copper Deflector for Improved Heat Balance

Removing heat more rapidly from the tube surface and restricting the arc plasma from impinging too far down the tube during welding also prevented excessive internal solidification voids associated with the welds. Several sets of split ring OFHC copper deflectors were used during welding thin wall 0.300 and 0.250-inch diameter tubing. The edge of the attached deflectors were located approximately 0.050 inch from the weld seam. Subsequent welds were found to exhibit more uniform and narrower weld beads.

5.6 Effects of Random Variables

Other random process variables which influenced weld metal quality were sodium proximity to the weld area and adequate grounding of the fuel rod during welding. Doping experiments proved that with minor amounts ($\sim$0.01 g) of sodium near the weld area, a high probability of weld blow holes or internal solidification voids resulted. Due to the relatively low melting temperature of sodium, it is easily vaporized and ionized at arc temperatures. Suddenly increasing easily ionized impurity constituents to the arc plasma

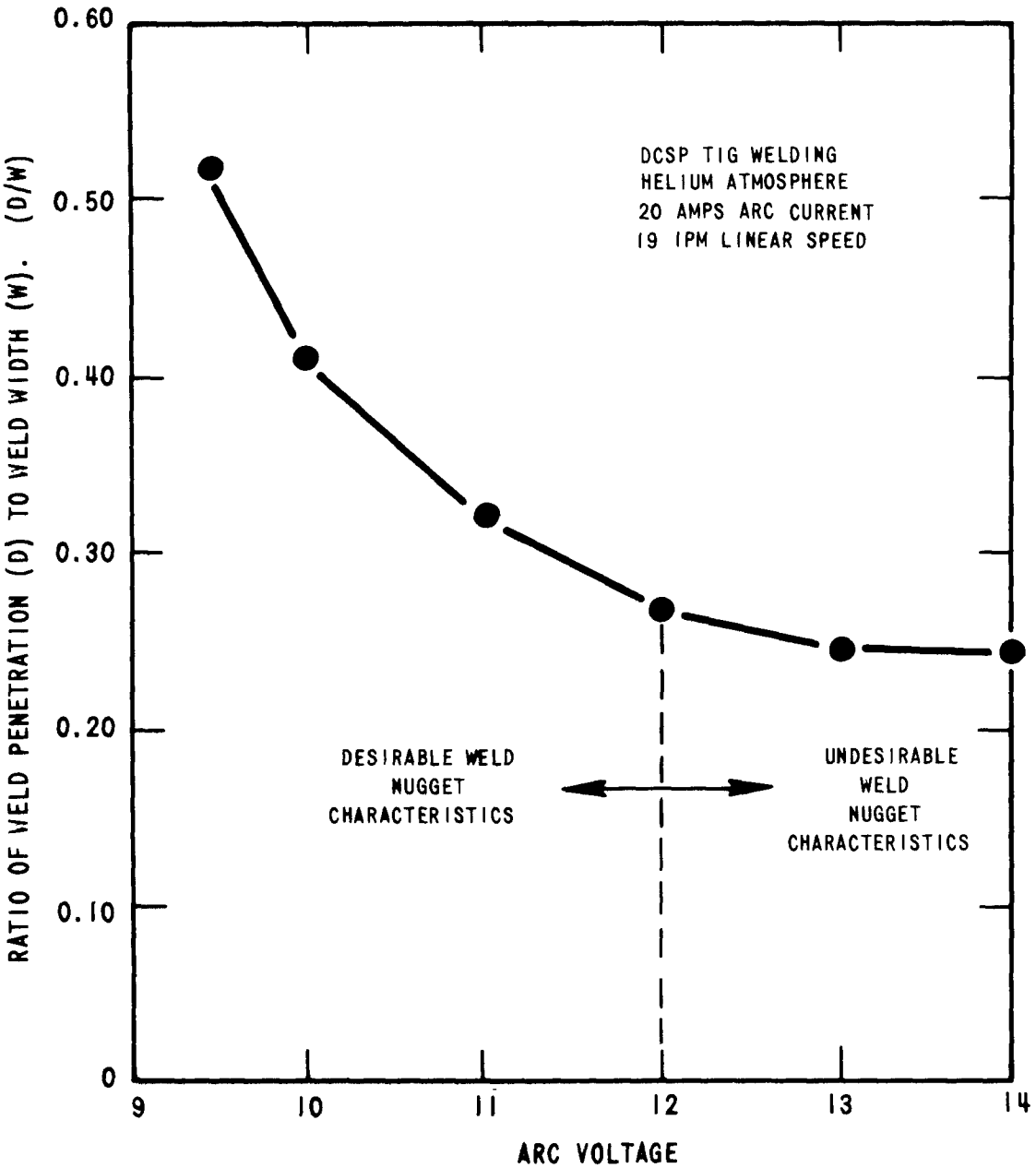

Figure 5 Effects of ARC Voltage on Weld Nugget Geometry

3462-5

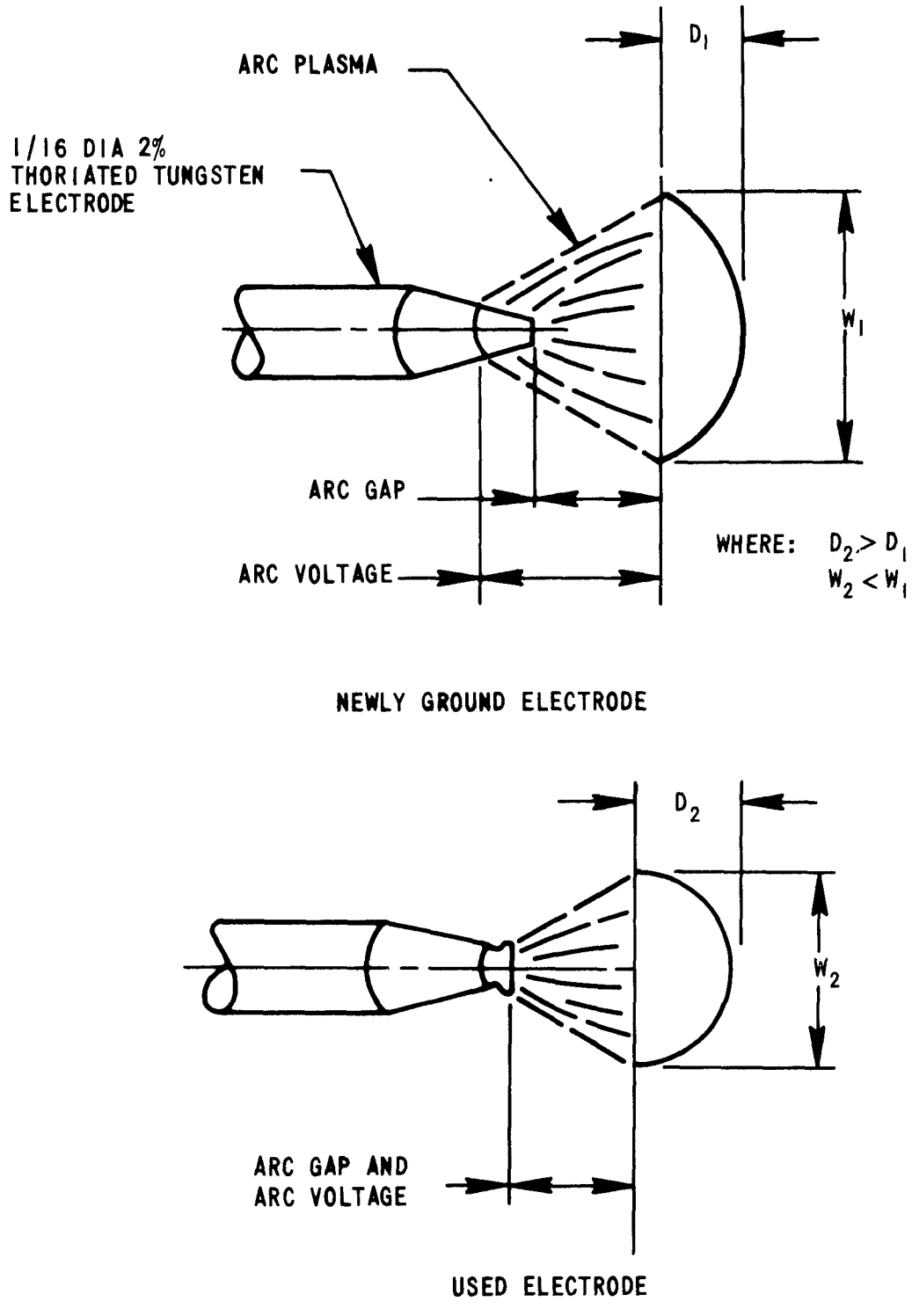

Figure 6 Schematic of ARC Characteristics as Influenced by Electrode Tip Geometry

3462-6

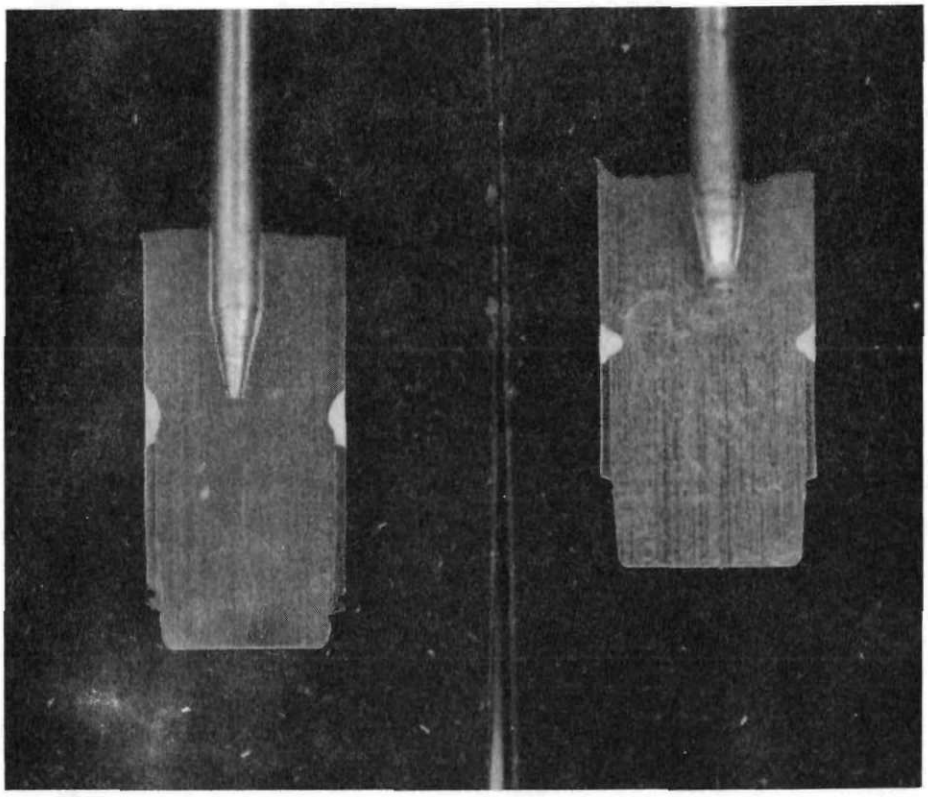

NOTE THE UNDESIRABLE WIDE,
FLAT WELD NUGGET RESULTING
FROM FRESHLY GROUND ELECTRODE
(LEFT)

Figure 7 Weld Nugget Geometry as Influenced by Electrode Tip Configuration in 0.010-in. Stainless Steel Tube to End Plug Welds

3462-7

results in causing variations to the anode spot size,[4] thus promoting the occurrence of defects. Defects of this nature were caused periodically during the welding of the top end plugs after loading the fuel pins with extruded sodium followed by a low temperature melting operation. An interesting problem occurred when a bottom end plug weld was discovered to have a gross internal solidification void after the fuel pellets were contained within the fuel pin and seated within sodium at 400°F. Samples processed simulating this condition and after a subsequent 1000°F sodium bonding treatment revealed significant different welding characteristics. Rewelding was normal after the 400°F seating operation, whereas all welds developed blow holes through which sodium slowly penetrated to the surface after the 1000°F bonding treatment. Wetting of the stainless steel is less effective at the lower temperature and apparently the 0.001 inch interference fit between end plug and tube prevents sodium migration to the weld area.

Adequate grounding of the fuel pin during welding proved to be a problem because of the thin walled tubing and possible contamination of the tubing outside diameter. Controlled experiments on mock-up specimens with a ground wire attached directly to the tube revealed weld bead widths decreased by 10-15% relative to samples not having a direct ground.

6. MATERIAL WELDABILITY

During the initial welding development, solution annealed 316 SS tubing from heat 1914 was used. The original welding procedure was changed from a single pass to a double weld pass technique prior to the fabrication of EBR-II fuel rods. The second pass was applied to remove internal solidification voids occasionally produced during the first weld cycle. Metallography of all development weld samples from heat 1914 which had been processed using a double weld pass failed to reveal any internal microfissures in any welds. Although metallography did reveal a random occurrence of internal solidification voids, Figure 8 illustrates schematically the formation of this type defect.

Because the last two fuel rods for EBR-II irradiation testing required 20% cold worked cladding, a formal qualification and weldability program was performed in order to verify the double pass welding procedure applied to solution annealed stainless steel tubing from heat 1914. Initial weldability results from heat 20303 revealed the presence of microfissures on the inner tube wall surface in the cast structure of 27% of the welds metallographically inspected. A photomicrograph is shown in Figure 9 of a 0.002 inch long microfissure emanating from an internal solidification void produced in a double pass weld. All microfissures evaluated were associated with various degrees of tube wall thinning due to internal weld metal solidification shrinkage.

In order to determine the mechanism of cracking associated with the welds in the cold worked tubing, various welding techniques were applied to separate groups of simulated weld mockups and the nondestructive and destructive inspection results analyzed. Analysis of welds made by a single pass technique revealed the presence of internal microfissures in 20% of the

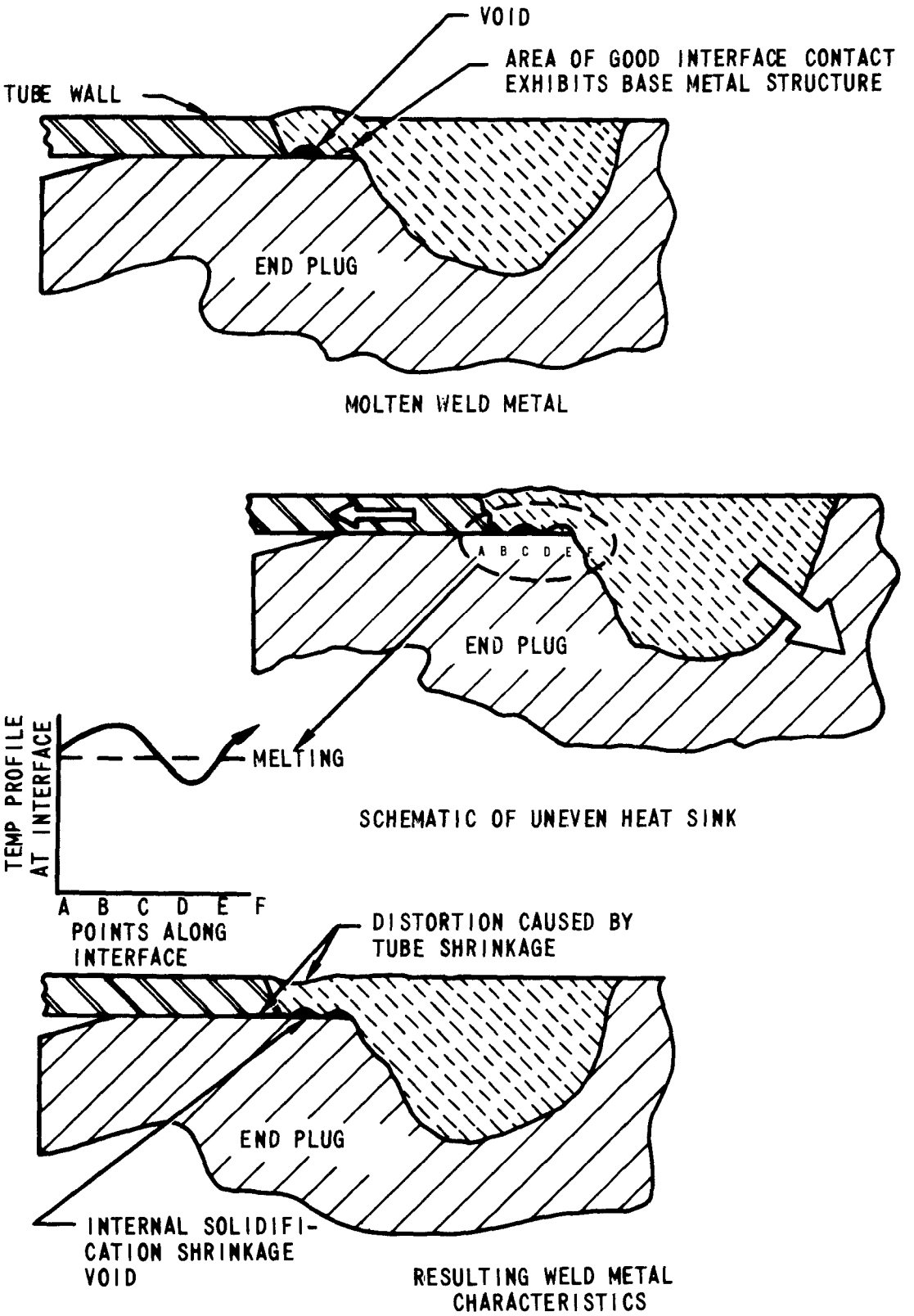

Figure 8 Effects of Weld Metal Cooling Rates on Solidification Shrinkage Void Formation

3462-8

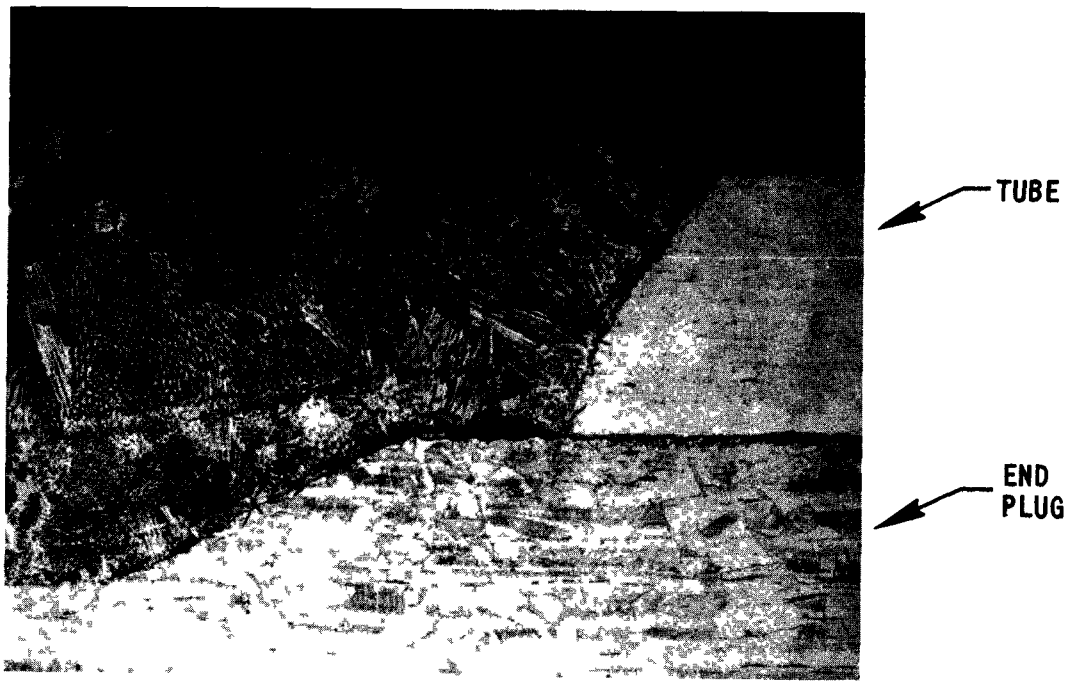

Figure 9 Photomicrograph Showing Longitudinal Section of Weld Nugget Containing a Typical Internal Microfissure Associated with a Solidification Void in 316 Stainless Steel, 20% Cold-Worked Tubing. Mag 125X

3462-9

welds metallographically inspected. All microfissures were associated with internal solidification voids greater than 50% of the tube wall thickness; single pass welds having solidification voids less than 50% of the tube wall thickness did not reveal any microfissures in the welds sectioned.

A multi-pass welding technique was then applied to a group of mockups and the results analyzed. The purpose of the multi-pass technique was to remove any detectable internal solidification voids, as determined radiographically, prior to metallographic sectioning. Analysis of these data revealed the presence of internal microfissures in 10% of the welds.

A comparative welding program, using fully-solution-annealed tubing from heat 20303, did not reveal any internal microfissures associated with equivalent size solidification voids in the resulting welds as determined metallographically.

Delta ferrite measurements were taken of all welds made during this program. No significant difference between groups or correlation with microfissure occurrence could be determined by the resulting delta ferrite measurements. These data ranged between 0.05 to 0.5% delta ferrite in the weld metal, as measured by a Magne-Gage. Calculations of nickel and chromium equivalents from the chemical compositions of end plug and tubing material indicated that all material fell within the fully-austenitic region of a modified stainless steel weld metal phase diagram by DeLong.[5] Points for the various materials used during the welding program are plotted in the diagram shown in Figure 10. Magne-Gage measurements on the as-received tubing and end plug material did not reveal any magnetic permeability which is consistent with the predicted composition.

Data derived from the welding program using 316 stainless steel tubing and end plug material tabulated in Table 1 indicate that air melt 20% cold worked tubing is more susceptible to internal microfissuring than solution annealed material of the same composition. The increased cracking tendency of the cold worked material is believed to be influenced primarily by two main factors: first, during weld metal solidification, the cold worked tubing imposes a higher stress in the area of microfissuring, and second, prior cold work can increase the energy of a grain boundary such that a shrinkage stress imposed in this area during solidification might decrease the grain boundary dihedral angle sufficiently to produce wetting by impurity solute atoms and subsequent hot cracking.[6,7]

Radiography was performed on all simulated mockup welds prior to sectioning. Film sensitivity levels of better than 2-2T were consistently achieved, although review of the radiographic film with corresponding weld samples exhibiting microfissures failed to reveal any evidence of these defects.

7. WELD DEFECTS

Weld defects encountered can be classified into six main categories: internal solidification voids, blow holes, microfissures, seams, underpenetration, and inclusions.

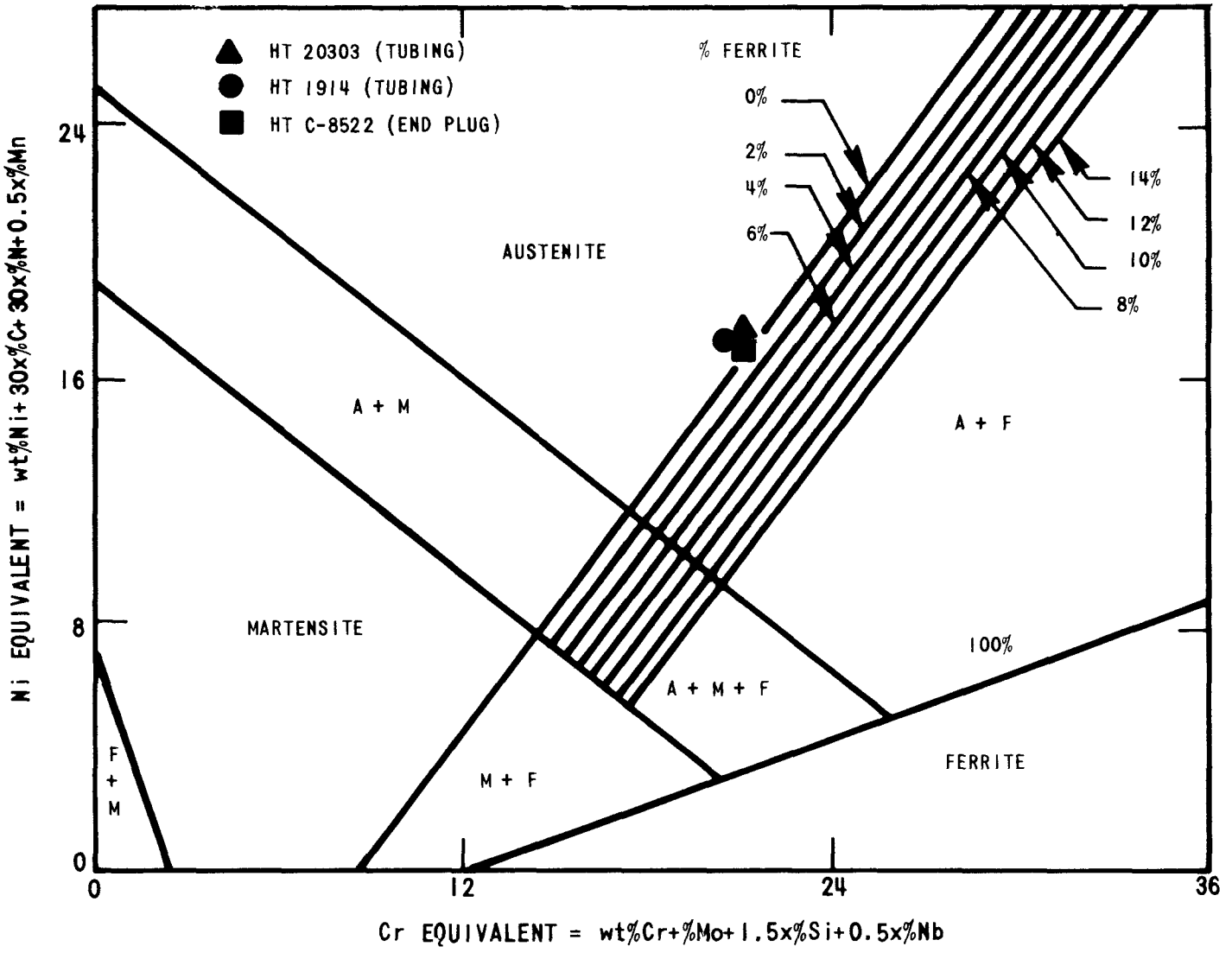

Figure 10 Revised Schaeffler Constitution Diagram for Stainless Steel Weld Metal

7.1 Internal Solidification Voids

This type defect was the most prominent. The circumferential length of these defects varied from very local (∿5%) to 50% of the weld circumference. Resulting reduction in wall thickness approached 90% of the original tube wall in some very severe cases. A longitudinal section of a weld exposing a transverse view of a typical internal solidification void is shown in Figure 9. As handling and end plug pressing procedures improved, the occurrence of these defects decreased; although when they were detected, their location was most often found in the weld overlap region. A photomacrograph shown in Figure 11 illustrates a severe example of an internal solidification void occurring in the weld overlap region. Radiography was used extensively for the detection of internal solidification voids.

7.2 Blow Holes

Initially, blow holes were encountered frequently in areas where poor localized fitup between tube and end plug occurred prior to welding. Blow holes occurred less frequently as processing procedures improved. However, when they did occur, the cause could generally be traced to minor amounts of sodium in or near the weld area. Visual, bubble testing, and helium leak test inspection were capable of detecting this type defect, depending on its size.

7.3 Microfissures

As discussed earlier, internal microfissuring was detected only in tubing which had been previously cold worked. By using controlled welding procedures, these defects could be eliminated. Metallography was the only method of inspection used to detect these defects. Surface fissures or crater cracks caused by improper weld current taper were rarely detected. A visual or penetrant inspection was used to detect surface defects.

7.4 Seams and Underpenetration

Evidence of seams and underpenetration occurred rarely. Seams were caused primarily by foreign material in the weld seam or poor grounding which would result in arc wander during welding. Underpenetration was primarily a function of weld program settings, speed control, and electrode positioning. Detection of seams was possible by visual, bubble test, and helium leak test inspection; underpenetration was detectable by radiography.

7.5 Inclusions

Two types of inclusions were noted: slag inclusions which appeared occasionally on the weld metal surface in the tail region, and small (∿1/32-inch) tungsten inclusions, from the electrode tip, occurring in approximately 3% of all welds. Removal of surface slag inclusions was performed by lightly abrading the surface, whereas tungsten inclusions required considerable local metal removal and subsequent weld repair. Radiography was unable to detect surface slag inclusions, whereas delineation of size and exact location of tungsten inclusions was easily identified.

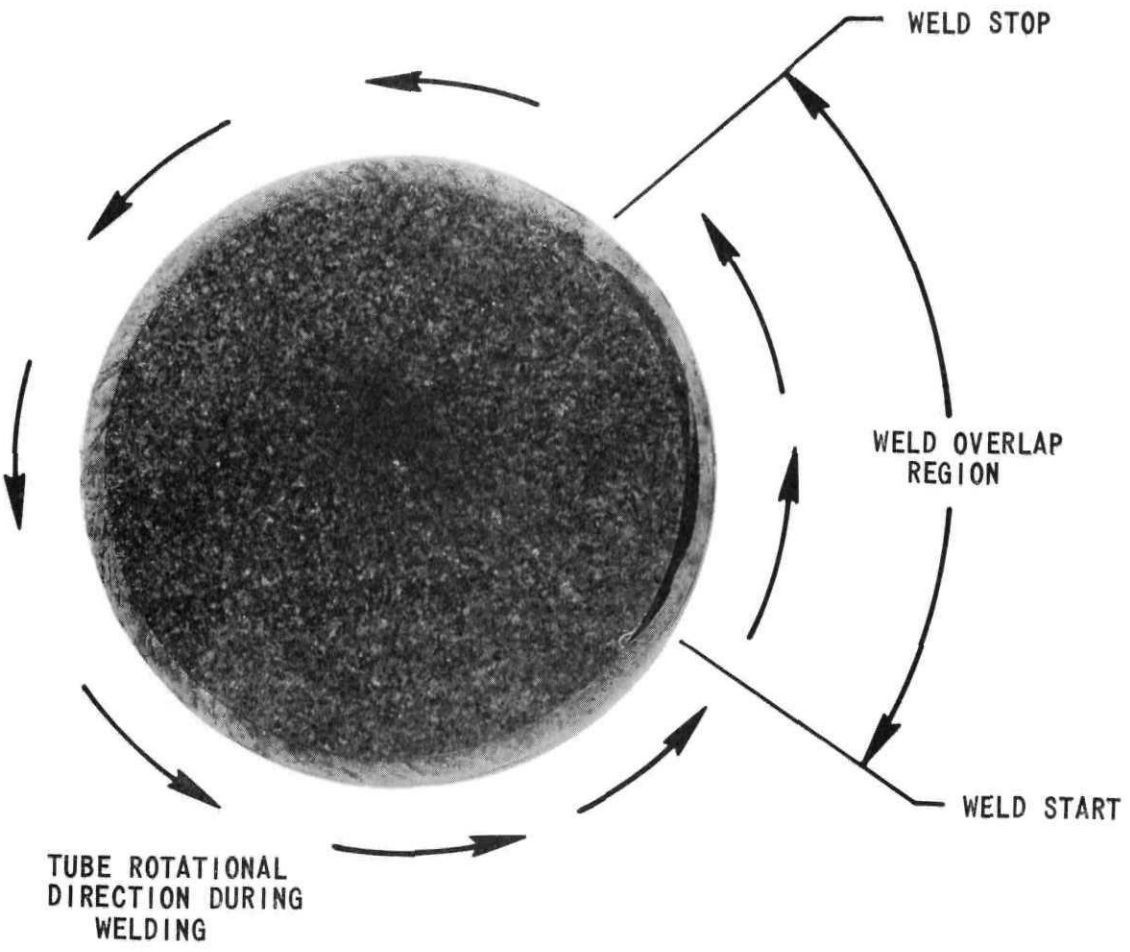

Figure 11 Tube to End Plug Closure Weld Showing the Circumferential Location of an Internal Solidification Void in the Weld Overlap Region. Mag 10X

3462-11

8. NONDESTRUCTIVE INSPECTION OF WELDS

Weld mockups were subjected to relevant nondestructive inspection tests, burst testing, and metallography. The nondestructive inspection tests were visual examination, alpha radioactivity monitoring, bubble testing, radiography, helium leak testing, dye penetrant testing, and dimensional inspection.

8.1 Visual and Radioactivity Monitoring

Prior to and immediately after removal of the plutonium-bearing fuel rods, the top welds were visually inspected for macro-type defects, i.e., blow holes and seams. Any evidence of defects necessitated a repair of that weld. Monitoring the top welds for levels of alpha contamination was performed immediately upon removal of the fuel rods from the welding chamber. Maximum acceptable levels of alpha contamination were:

<2500 D/M (fixed)
<500 D/M average per 100 cm^2 (fixed)
<10 D/M per 100 cm^2 (smearable)
(Note: D/M indicates disintegrations per minute)

Some fuel rod top welds that had been improperly decontaminated exceeded these limits. Lightly abrading the weld face reduced locally contaminated areas to the allowable limits.

8.2 Bubble Testing

This inspection test was performed on all plutonium-bearing fuel rods immediately after alpha monitoring. The procedure consisted of subjecting the entire fuel pin to helium at 100 psig external pressure for one-half hour, then immediately submerging the top end closure weld in ethyl alcohol. Any evidence of bubbles emanating from the weld was cause for rejection. This test exposed several small weld defects which were undetected by visual examination. Acceptable results from bubble testing was required prior to further processing of the fuel rods in the noncontaminated sodium laboratory.

8.3 Radiography

Radiographic inspection was performed on all top and bottom fuel rod end closure welds. Four different radiographic views (0°, 45°, 90°, and 135°) were taken of each weldment. Film sensitivity levels of better than 2-2T were required and verified by a radiographic penetrameter and a defect standard. A print of a typical weld radiograph is shown in Figure 12. The defect standard was fabricated from the same tubing and end plugs used during pin fabrication. Indications which appear in the figure represent simulated defects; they are (from left to right): (1) unwelded seam formed by pressing the end plug and tube, (2) a 0.002-inch deep groove machined into the inside diameter of the tube, and (3) a 0.004-inch deep groove machined into the inside diameter of the tube. Shape correction blocks[8] consisting of holes drilled through a stainless steel flat plate were used for all fuel rod weld radiographs. This form converts the cylindrical rod into a flat plate which results in uniform subject density and contrast

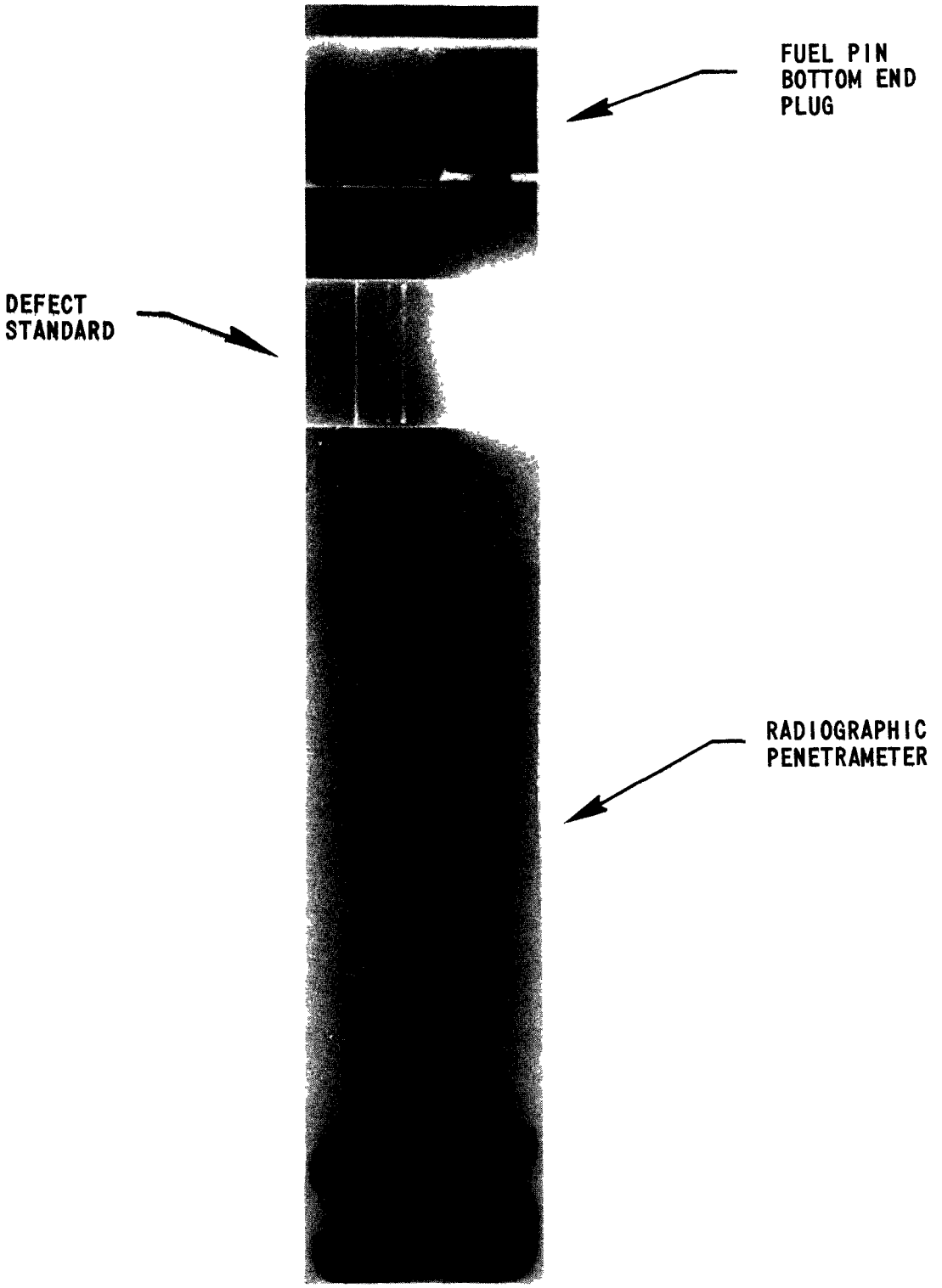

Figure 12 Positive of a Weld Radiograph Illustrating an Acceptable Bottom End Closure Weld. Note the Small Fuel Chip Between Bottom Insulator and Clad ID. Mag 3X

3462-12

which improves defect clarity. Using these radiographic techniques, 0.001-inch high internal solidification voids were detectable. A 0.001-inch high defect represents < .3% of the total correction block thickness, but, significantly, 10% of the fuel rod clad thickness. Radiographic inspection techniques developed were capable of detecting all weld defects described earlier with the exception of weld metal microfissures. Fuel rod end closure welds were rejected after radiography if they revealed < 100% weld penetration, evidence of metallic or nonmetallic inclusions, detectable internal solidification voids, or porosity. Internal solidification voids were the defect type most commonly encountered during fuel rod fabrication.

8.4 Helium Leak Testing

All bottom fuel rod welds were helium leak tested by evacuating the open ended tube and spraying helium on the external surface. Inspection of final end closure fuel rod welds, after final fuel rod processing, was performed by subjecting the entire fuel rod to helium at 100 psig external pressure for one-half hour, evacuating the container surrounding the fuel rod, and monitoring the leak rate. All fuel rod closure welds were inspected to a maximum acceptable leak of 1×10^{-8} cc/sec. No leaks exceeding this value were detected on actual fuel bearing rods, although some weld mockups did reveal small communicable defects which violated the maximum acceptable leak.

8.5 Dye Penetrant Inspection

Penetrant testing of all welds was performed to insure surface weld metal integrity. Initial weld mockups revealed minor surface indications emanating from small crater cracks. This problem was eliminated by removing several capacitors from the capacitor bank within the power supply.

8.6 Dimensional Inspection

Resulting weld bead diameters were dimensionally inspected to insure that all welds did not extend >0.003-inch beyond the tube outside diameter. Generally, welds requiring more than two passes violated this requirement as axial fuel tube shrinkage resulted in additional cast metal in the weld area.

9. CONCLUSIONS

Hermetically-sealed irradiation fuel rods containing (U,Pu)C fuel pellets immersed in sodium with mechanically and metallurgically sound weld joints between thin wall austenitic stainless steel tubing and end closures have been obtained by the tungsten inert gas (helium) process. Special attention was required of seemingly unimportant process and welding variables to achieve acceptable end closure welds. This development work resulted in the documentation of a welding specification which is presented in Appendix A. The following conclusions were established from this development work.

1. Weld defects formed in thin wall austenitic stainless steel tubing to end closures are primarily caused by improper component handling and cleaning, end closure pressing, electrode positioning and shape, copper deflector location, and equipment malfunctions.

2. Minor amounts of sodium near the weld joint causes variations to the anode spot size by ionizing the sodium at arc temperatures which results in defective welds.

3. Internal weld metal microfissures were only detected in air melted, 20% cold worked 316 stainless steel tubing. All microfissures were associated with internal solidification voids of various sizes.

4. Delta ferrite content in the as-cast weld metal ranged from 0.05 to 0.5%.

5. Nondestructive inspection methods applied during this development work were capable of detecting all types of weld defects encountered except the small internal microfissures in the weld metal.

10. ACKNOWLEDGEMENTS

Welding development and fabrication work was conducted in performance of AEC Contract AT(30-1)-3791.

The authors gratefully acknowledge the assistance of employees at Westinghouse Advanced Reactors Division Plutonium Laboratory: Welding Equipment Installation and Operation, P. F. Simpson and R. C. Savakes; Nondestructive Inspection, W. B. Bargerstock.

REFERENCES

1. P. J. Levine, "Thermal Flux Irradiation Studies of (U,Pu)C Fuel Design, Fabrication and Reactor Insertion of Fuel Pins and Capsules," WARD-3791-16, April 1969.

2. A. Biancheria, E. C. Bishop, and W. R. Jacoby, "Uranium Plutonium Carbide Development Quarterly Progress Report," WCAP-3791-10, September 30, 1967.

3. W. R. Savage, S. S. Struck, and Y. Yshakowg, "The Effects of Electrode Geometry in TIG Welding," Welding Journal, 45, (12), Research Suppl., pp. 489-496 (1965).

4. H. C. Ludwig, "Current Density and Anode Spot Size in the Gas Tungsten Arc," Welding Journal, 47 (5), Research Suppl., pp. 234-240 (1968).

5. W. T. DeLong, "A Modified Phase Diagram for Stainless Steel Weld Metals," Metals Progress, 77 (2), pp. 98-100 (1960).

6. D. McLean, "Grain Boundaries - Part 1. Explanation of Microstructures in Terms of Energies," Metal Treatment and Drop Forging, 23, pp. 3-10 January 1956.

7. F. C. Hull, "Effect of Delta Ferrite on Hot Cracking of Stainless Steel," Welding Journal, 46 (9), pp. 399-409, September 1967.

8. A. E. Oaks, "Radiographic Inspection of Nuclear Core Materials and Components," ASTM Special Technical Publication No. 223, pp. 304-318 (1957).

APPENDIX A

EBR-II, PHASE I
FUEL IRRADIATION PIN WELDING PROCEDURE

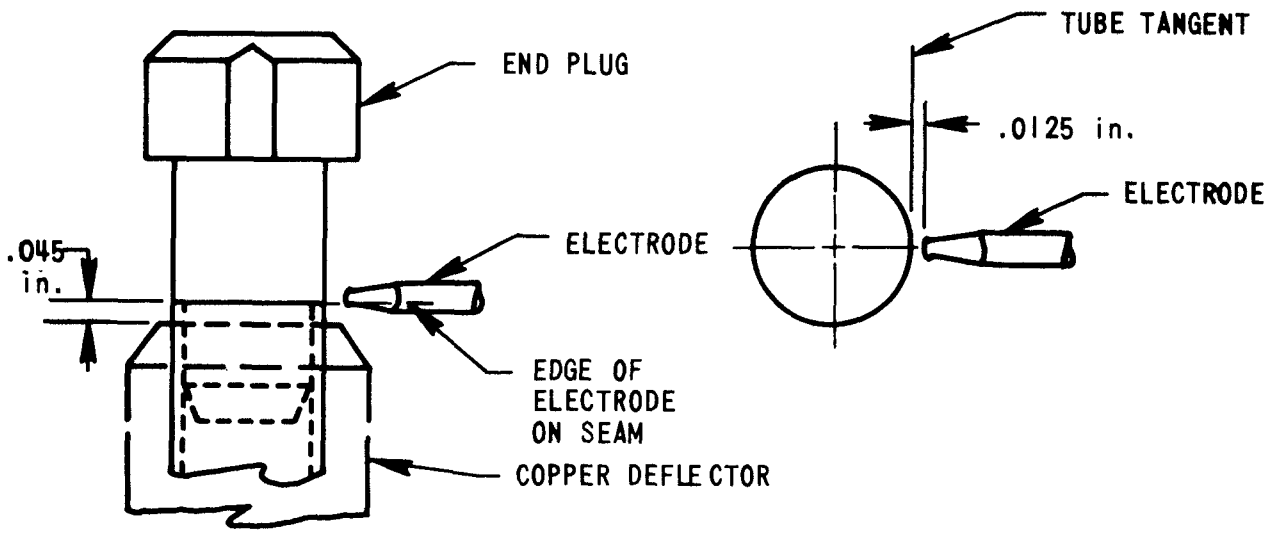

3462-13

SCOPE

This procedure defines the materials, equipment, welding parameters, and welding conditions to be used during the fabrication of the top and bottom end plug weldments on all EBR-II irradiation fuel pins. This procedure is in accordance with the requirements defined in Westinghouse Dwg. 883D275.

EQUIPMENT

1. Miller Model ESR-150 amp power source.
2. Vacuum chamber capable of evacuation to $\leq$.03μ Hg and having a static leak rate of $\leq$ 1μ/min.
3. Jacobs chuck, and suitable drive for holding tubes during welding.
4. Fixed electrode holder.
5. Ultra-pure helium with total $O_2 + N_2$ <5ppm.

MATERIALS

1. Top and bottom end plugs - 316 SS according to ASTM-A-276
2. 304 SS solution annealed fuel tubes (.300" O.D. x .010" & .012" wall) according to ARD-AMMA-001-1.
3. 316 SS solution annealed fuel tubes (.300" O.D. x .250" O.D. x .010" & .012" wall) according to ARD-AMMA-001-2.
4. 316 SS, 20% cold worked fuel tubes (.300" O.D. x .012" wall) according to ARD-AMMA-001-2.

MACHINE SETTINGS

1. All welding will be performed in a welding chamber backfilled with ultra-pure helium after a minimum four-hour evacuation to $\leq .03\mu$ Hg with a resulting static leak rate of $\leq 1\mu$/min.

2. No. 562 slope generator module:

   a. Hot start
   b. Up slope rate: 0
   c. Up slope time: 0
   d. Initial current: 30 on dial
   e. Decay rate: 0

3. Weld current lock: 20A

4. No. 563 electronic timer module: 4 seconds

5. Control set for "Local" and "Automatic."

6. No. 564 finish slope module:

   a. Transition current: 20
   b. Rate: 80 on dial
   c. Time: 2 seconds
   d. Hold current: 0

7. Impulse Arc Starter

   a. Reverse polarity
   b. 40% intensity

8. Electrode: 2% thoriated, 1/16 diameter tungsten, D/4 tip with a 60° included angle (seasoned). Position as shown in sketch.

9. Speed: 20 rpm (19 ipm) for .300" O.D. tubing
   24 rpm (19 ipm) for .250" O.D. tubing

10. Arc gap: .0125"

WELDING PROCEDURE

1. Check rotational speed for one minute.

2. Set machine settings and run through on no weld program.

3. Load clean components into chamber, evacuate and backfull according to No. 1 under "Machine Settings." Make atmosphere check weld on dummy SS pin. Resulting weld must be bright and shiny.

4. Press end plugs inside welding chamber. Insert tube assembly within Jacobs chuck, indicate runout near weld seam, .002" maximum TIR before welding.

5. Position electrode, weld chill, and set arc gap (during rotation).

6. Start rotation, initiate welding program on Miller welder, and weld. *Reposition the electrode down .005" relative to the first pass and weld a second pass. Observe and note any unusual characteristics during welding.

7. In the event of the occurrence of any holes or pell-backs, notify engineering for repair instructions.

8. Unload components after a suitable cool-down period. Health Physics must check for excessive α-contamination. Route fuel pins to bubble test inspection.

---

*Note: For all 20% cold worked 316 SS tubing, only a single pass will be allowed.

EXTERNAL DISTRIBUTION LIST

U. S. ATOMIC ENERGY COMMISSION

Division of Reactor Development and Technology
Washington, D. C. 20545

Assistant Director, Engineering Standards
Assistant Director, Nuclear Safety
Assistant Director, Plant Engineering
Assistant Director, Program Analysis
Assistant Director, Project Management (2)
Assistant Director, Reactor Engineering (2)
Assistant Director, Reactor Technology
Chief, Fuels and Materials Branch (3)
Chief, Fuel Engineering Branch
Chief, Reactor Vessels Branch

Division of Naval Reactors
Chief, Nuclear Materials Branch
United States Atomic Energy Commission
Washington, D. C. 20545

New York Operations Office
Manager (2)
U. S. Atomic Energy Commission
376 Hudson Street
New York, New York 10014

Division of Technical Information Extension (3)* (50)**
United States Atomic Energy Commission
P. O. Box 62
Oak Ridge, Tennessee 37831

Office of Assistant General Council for Patents
U. S. Atomic Energy Commission
Washington, D. C. 20545

Assistant Director Pacific Northwest Laboratory
U. S. Atomic Energy Commission
P. O. Box 550
Richland, Washington 99352

AEC-RDT Site Offices
Argonne National Laboratory
U. S. Atomic Energy Commission
Building 2
Argonne, Illinois 60439

---

* Submitted with transmittal form AEC-426
** Submitted for transmittal to recipient under UKAEA/USAEC and EURATOM/USAEC Fast Breeder Reactor Information Exchange Arrangements

Argonne National Laboratory
U. S. Atomic Energy Commission
P. O. Box 2108
Idaho Falls, Idaho 83401

Atomics International
U. S. Atomic Energy Commission
P. O. Box 1446
Canoga Park, California 91304

General Electric Company, NSP
U. S. Atomic Energy Commission
P. O. Box 15132
Cincinnati, Ohio 45215

General Electric Company
U. S. Atomic Energy Commission
310 DeGuigne Drive
Sunnyvale, California 94086

Gulf - General Atomic
U. S. Atomic Energy Commission
P. O. Box 2325
San Diego, California 92112

Oak Ridge National Laboratory
U. S. Atomic Energy Commission
P. O. Box X
Oak Ridge, Tennessee 37830

Pacific Northwest Laboratory
U. S. Atomic Energy Commission
P. O. Box 550
Richland, Washington 99352

Westinghouse Electric Corporation (2)
U. S. Atomic Energy Commission
Advanced Reactors Division
P. O. Box 158
Madison, Pennsylvania 15663

LABORATORIES

Director, LMFBR Program Office (2)
Argonne National Laboratory
9700 South Cass Avenue
Argonne, Illinois 60439

Director, Metallurgy Division (2)
Argonne National Laboratory
9700 South Cass Avenue
Argonne, Illinois 60439

Manager, FFTF Project (2)
Pacific Northwest Laboratory
P. O. Box 999
Richland, Washington 99352

FFTF Fuels Department (2)
Pacific Northwest Laboratory
P. O. Box 999
Richland, Washington 99352

Manager, Chemistry and Metallurgy Division
Pacific Northwest Laboratory
P. O. Box 999
Richland, Washington 99352

Division Leader, Chemistry and Metallurgy Division (CMB)
Los Alamos Scientific Laboratory
P. O. Box 1663
Los Alamos, New Mexico 87544

Director, Metallurgy and Materials Science Division
Brookhaven National Laboratory
Upton, New York 11973

Director, Metals and Ceramics Division (2)
Oak Ridge National Laboratory
P. O. Box X
Oak Ridge, Tennessee 37830

Division Chief, M & S Division
NASA - Lewis Research Center
21000 Brookpark Road
Cleveland, Ohio 44135

Director, Atomics International
Liquid Metal Engineering Center
P. O. Box 309
Canoga Park, California 91304

Division Leader, Inorganic Materials
Chemistry Department
Lawrence Radiation Laboratory
P. O. Box 808
Livermore, California 94551

Manager, Advanced Development Activity
General Electric Company
Knolls Atomic Power Laboratory
P. O. Box 1072
Schenectady, New York 12301

General Manager, Westinghouse Electric Corporation
Bettis Atomic Power Laboratory
P. O. Box 79
West Mifflin, Pennsylvania 15122

CONTRACTORS

Director, LMFBR Technology Program
Atomics International
P. O. Box 309
Canoga Park, California 91304

Associate Manager, Materials Engineering Department
Battelle Memorial Institute
Columbus Laboratories
505 King Avenue
Columbus, Ohio 43201

Director, Nuclear Development Center
The Babcock and Wilcox Company
Atomic Energy Division
Lynchburg, Virginia 24501

Manager, Nuclear Laboratories
Combustion Engineering, Inc.
Nuclear Division
Prospect Hill Road
Windsor, Connecticut 06095

Laboratory Assistant Director
Gulf-General Atomic
P. O. Box 608
San Diego, California 92112

Manager, Plutonium Chemistry and Ceramics Fuels Development
Plutonium Laboratory
Nuclear Materials and Equipment Corporation
Leechburg, Pennsylvania 15656

Manager, Sodium Reactor Technology
General Electric Company
Breeder Reactor Development Operation
210 DeGuigne Drive
Sunnyvale, California 94086

Manager, Research, United Nuclear Corporation
Research and Engineering Center
Grasslands Road
Elmsford, New York 10523

Head, Fuels and Materials
Atomic Power Development Associates
1911 First Street
Detroit, Michigan 48226

K-2 Group Leader
Reactor Division
Los Alamos Scientific Laboratory
P. O. Box 1663
Los Alamos, New Mexico 87544

Irradiations Manager
EBR-II Project
Argonne National Laboratory
P. O. Box 1096
Idaho Falls, Idaho 83401

Director, Vallecitos Nuclear Center
General Electric Company
P. O. Box 846
Pleasanton, California 94566